ISBN: 978-3-95450-241-7 ISSN: 2673-5350 doi:10.18429/JACoW-IBIC2022-MOP18

X-RAY PINHOLE CAMERA SPATIAL RESOLUTION USING HIGH ASPECT RATIO LIGA PINHOLE APERTURES

N. Vitoratou*, L. Bobb, Diamond Light Source, Oxfordshire, UK
G. Rehm, Helmholtz-Zentrum für Materialien und Energie, Berlin, Germany
A. Last, Karlsruhe Institute of Technology, Karlsruhe, Germany

Abstract

X-ray pinhole cameras are employed to provide the transverse profile of the electron beam from which the emittance, coupling and energy spread are calculated in the storage ring of Diamond Light Source. Tungsten blades separated by shims are commonly used to form the pinhole aperture. However, this approach introduces uncertainties regarding the aperture size. X-ray lithography, electroplating and moulding, known as LIGA, has been used to provide thin screens with well-defined and high aspect ratio pinhole apertures. Thus, the optimal aperture size given the beam spectrum can be used to improve the spatial resolution of the pinhole camera. Experimental results using a LIGA screen of different aperture sizes have been compared to SRW-Python simulations over the 15 – 35 keV photon energy range. Good agreement has been demonstrated between the experimental and the simulation data. Challenges and considerations for this method are also presented.

INTRODUCTION

X-ray pinhole cameras (XPCs) are a well-established diagnostic tool for measurement of the 2D transverse beam profile of the electron beam in the storage ring [1]. From the acquired beam size measurement, combined with knowledge of the lattice parameters, the emittance and coupling are calculated. The expected beam sizes in Diamond-II will be smaller than the nominal operation of Diamond, particularly for emittance measurement of the squeezed beam after correction of the lattice using the linear optics from closed orbits (LOCO) method [2].

The Point Spread Function (PSF) of the imaging system should be minimised to improve the spatial resolution. The overall PSF is represented by the contributions of the scintillator screen, the lens, the camera sensor and the pinhole aperture itself which is a fundamental component in the pinhole camera. Reduction of the PSF can be achieved by using the optimal pinhole aperture size for the given photon beam energy of the synchrotron radiation [1]. For sufficient contrast at photon energies in the 15 – 60 keV range, the pinhole aperture must be formed using a material with a high atomic number.

High Z-number materials are often difficult to machine, especially to form high aspect ratio structures, e.g. a rectilinear square aperture of 10 µm × 10 µm with a thickness of 250 µm to 1 mm. Due to this, the pinhole aperture is often formed by stacking two orthogonal sets of tungsten blades separated by precisely machined shims. The thickness of the shims between the tungsten blades sets the aperture size [3]. Although the blades have surfaces that are easy to polish and the shims can be manufactured to the specified thickness, there are drawbacks to this stacked design. Firstly the pinhole aperture, which from theory should be an infinitesimally thin screen is a 10 mm long tunnel, making simulation challenging. Secondly, the effective aperture size is typically larger than the shim thickness. And thirdly, the absolute measurement of the effective aperture size in this geometry is not trivial.

LIGA (X-ray lithography) technology [4] enables the fabrication of high-aspect ratio structures using high-Z materials such that the pinhole aperture size is known and controllable. Furthermore, the tunnel-like geometry of the aperture is removed to provide better agreement with theoretical models. At the Karlsruhe Institute of Technology, unique LIGA screens are produced. These are made from gold with a thickness up to 250 µm. Thus, allowing the comparison between simulations of the pinhole camera with real acquired data on the accelerator. This could enable simulation of the PSF of the pinhole camera instead of PSF measurement using Touschek calibration with beam which is time-consuming [5].

In this paper, simulations and measured pinhole camera images from a bending magnet sourcepoint using a LIGA screen are compared.

EXPERIMENTAL SETUP

Pinhole camera 3 is installed on the Diagnostics X-ray beamline inside the storage ring tunnel for the purpose of R&D. A schematic of the setup is shown in Fig. 1. The pinhole-to-scintillator distance is 9.72 m, the source-to-

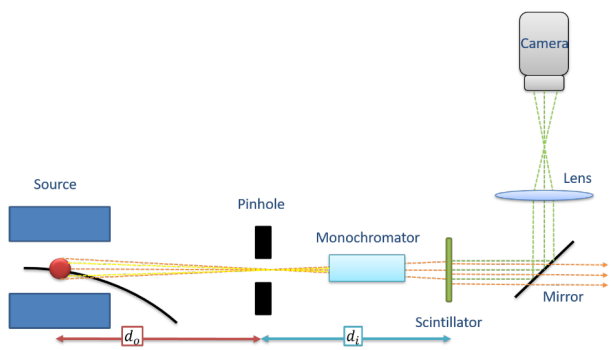

Figure 1: Schematic of an X-ray pinhole camera from a bending magnet sourcepoint.

* niki.vitoratou@diamond.ac.uk

ISBN: 978-3-95450-241-7 ISSN: 2673-5350 doi:10.18429/JACoW-IBIC2022-MOP18

pinhole magnification was measured as 2.54, the source-to-pinhole distance is 3.82 m and the scintillator-to-camera magnification was measured as 1.02. Approximately 1 m upstream of the scintillator is a multilayer monochromator. The bandwidth of the Mo/Si multilayer monochromator is < 1 keV [6]. The parameters of the multilayer monochromator are summarised in Table 1.

Table 1: Multilayer Monochromator Parameters

Parameter	Value
Mirror dimensions	300 mm × 50 mm
d-spacing	4.8 nm
Coating	Mo/Si
Substrate	Float glass
Number of layer-pairs	100

A side effect of multilayer monochromator on micro-imaging applications is the stripe pattern induced in the image [6]. On the Diagnostics X-ray beamline the monochromator reflects in the horizontal plane to ensure that the vertical dimension of the imaged beam profile is not distorted by this well-known banding effect. The single bounce monochromator means it is necessary to track the reflected beam with a camera mounted on translation stages. At 12 keV, the Bragg angle is ≈ 0.67 degree, which gives a beam-deflection of ≈ 23 mm at a distance of 1 m.

Figure 2 shows the design for the LIGA pinhole screen. The screen features square apertures with sizes ranging from 10 µm to 50 µm. For each aperture size there is a 3×3 grid of apertures. The apertures are separated to ensure independent images are obtained from each pinhole. A 400 µm aperture is included for initial alignment. Each pinhole aperture size was checked using a scanning electron microscope (SEM) to verify the size. Differences in the range of few microns were revealed between the measurement and the specification. This was taken into account for the comparison studies between experiment and simulation.

SIMULATION

The Synchrotron Radiation Workshop in Python (SRW-Python) [7, 8] was used to simulate the image of the photon beam at the scintillator screen. The simulation settings were defined according to the experimental setup. Firstly, the SR emitted from a single electron sourcepoint propagated through a square pinhole aperture was simulated for a fixed photon energy. This was then extended using the partially coherent wavefront propagation for 2000 individual electrons with a Gaussian distribution representing the electron beam profile.

The procedure was repeated for a set of energies from 15 – 35 keV for each pinhole aperture size. The simulation assumes X-rays propagate in vacuum, therefore the 1 mm aluminium window from vacuum-to-air and 10 m air are omitted. The monochromator was also omitted from the simulation since the photon energy is specified.

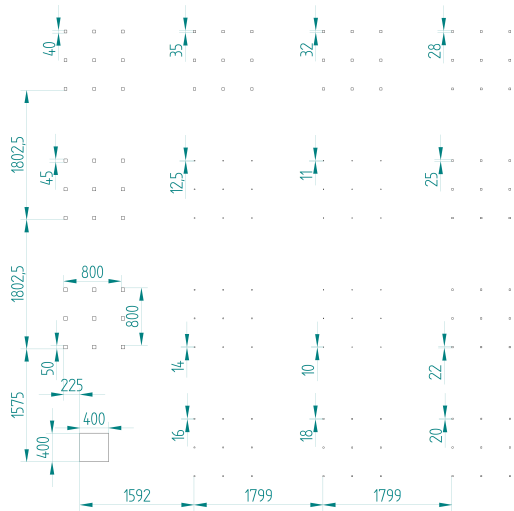

Figure 2: Pinhole screen design of 3x3 arrays of square holes.

The simulated beam intensity data from SRW was used to construct the 2D image of the beam on the scintillator screen. The image was convolved with the scintillator screen PSF which was measured experimentally using the knife edge method. The vertical projection of the beam on the scintillator screen was fitted with a 1D Gaussian fit and the sigma provided the vertical beam size on the scintillator screen.

PINHOLE APERTURE MEASUREMENTS

Figure 3 shows an image acquired using the LIGA screen with the monochromator retracted (i.e., with white beam). Some leakage is seen of the SR fan through the ≈ 250 µm thick LIGA screen. Images were then acquired for a range of

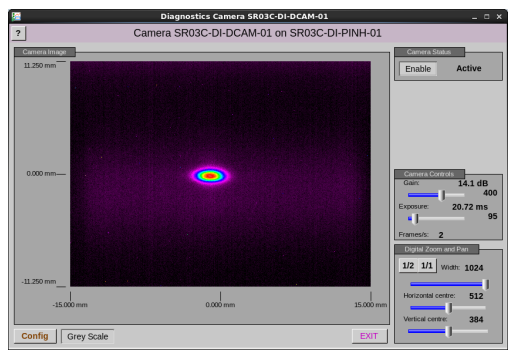

Figure 3: White beam image using the LIGA screen.

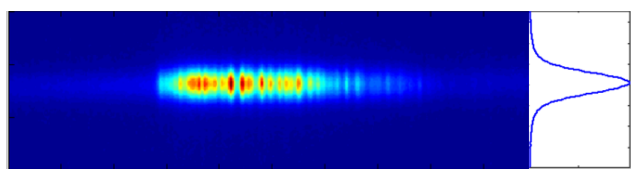

Figure 4: Image from the pinhole camera at 23 keV using a 25 µm aperture.

ISBN: 978-3-95450-241-7 ISSN: 2673-5350 doi:10.18429/JACoW-IBIC2022-MOP18

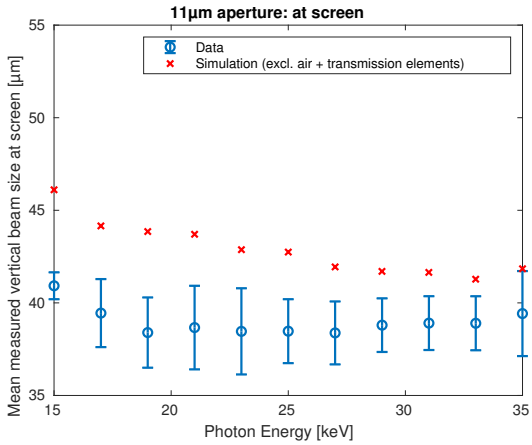

(a) 11 µm aperture.

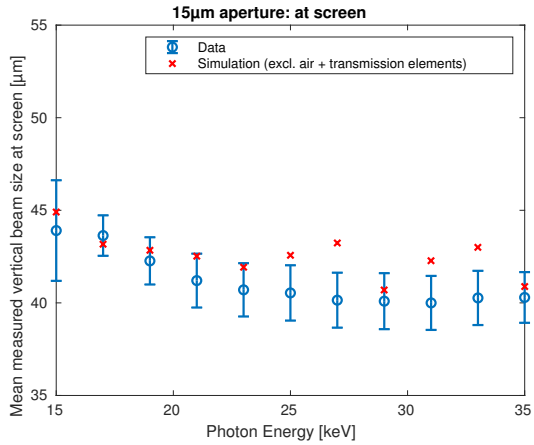

(b) 15 µm aperture.

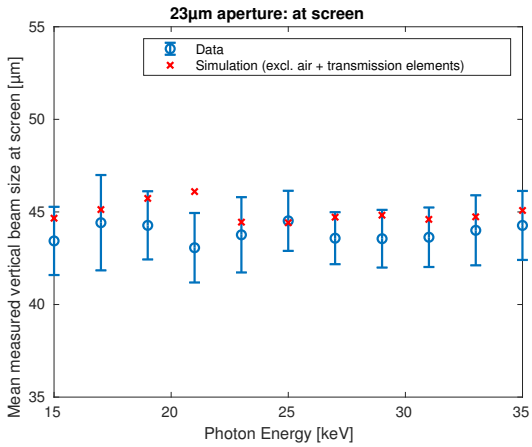

(c) 23 µm aperture

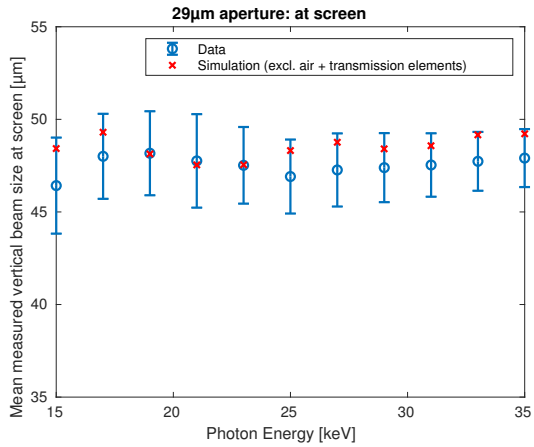

(d) 29 µm aperture

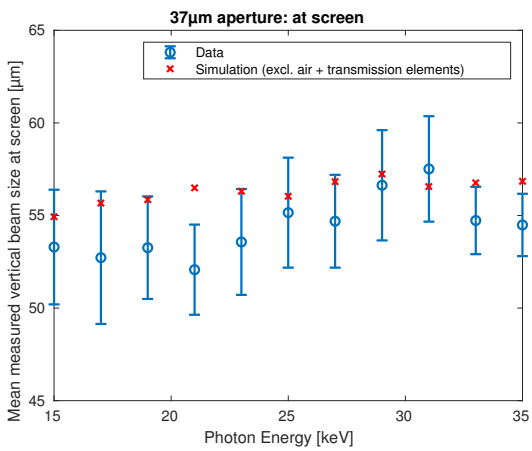

(e) 37 µm aperture

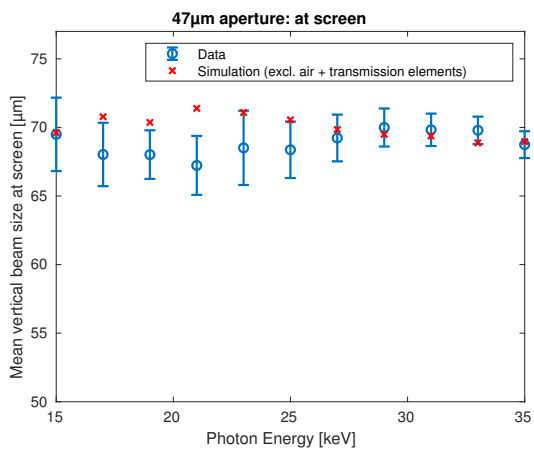

(f) 47 µm aperture

Figure 5: Comparison of simulation and experimental data for different LIGA pinhole aperture sizes and photon energies.

photon energies using different aperture sizes. A typical image is shown in Fig. 4. The expected stripe pattern from the multilayer monochromator is observed, however the vertical profile of the beam is preserved in the image.

The vertical beam size was measured by stacking five images from the pinhole camera. Hot pixels were removed using a median filter. Due to the stripe pattern, each column of the stacked image was fitted with a 1D double Gaussian profile, where one of the Gaussian curves represents the beam profile while the second Gaussian describes the background.

To ensure reasonable fits, a signal-to-noise threshold was applied to only include columns where the Gaussian peak that represents the beam profile was 20 times greater than

ISBN: 978-3-95450-241-7 ISSN: 2673-5350 doi:10.18429/JACoW-IBIC2022-MOP18

the average background. The average background was taken from a corner of the image where the SR fan intensity was significantly reduced. The background in the region of the image is significantly greater than the obtained average background, thus a threshold factor of 20 was found to be most appropriate.

The experimental data for a range of aperture sizes is shown in Fig. 5. For each data point the average measured vertical beam size is presented with an error bar of the standard deviation from the Gaussian fits of the columns of the image. The vertical beam size at the scintillator screen is compared over a range of photon energies from 15 – 35 keV. The standard deviations range from a few per cent up to 10% with respect to the average measured beam size at each photon energy.

EXPERIMENT AND SIMULATION COMPARISON

The experiment and simulation data comparison was conducted for different aperture sizes from 11 to 47 µm as shown in Fig. 5. The aperture size used as the label in the plots is according to the SEM measurements and not the specification.

The relative difference between the simulated and experimentally measured beam sizes over a range of photon energies for each aperture is summarised in Fig. 6. For most cases, the mean value of the relative difference across the energy range for each aperture size is below 5% with the highest value being 8%, excluding the 11 µm dataset.

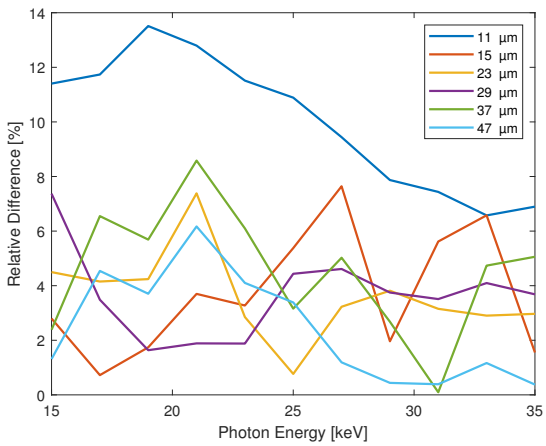

Figure 6: Relative difference between the simulated and measured beam sizes over a range of photon energies for each aperture size.

It should be noted that a small degree of disagreement was expected since the simulation uses a bare lattice and assumes perfectly monochromatic light, whereas the data was acquired from the synchrotron with insertion devices at gaps for nominal user beam and the multilayer monochromator has finite bandwidth. Also, the photon absorption in the aluminium window from vacuum-to-air and the 10 m air were not included in the simulation.

For the 11 µm aperture the relative difference between the simulated and measured beam sizes is much higher in comparison to the other apertures. This discrepancy may arise from the quality of the 11 µm apertures, which were observed to be visually poorer under the SEM, since these apertures approach the aspect ratio limit of the LIGA fabrication process.

CONCLUSIONS

LIGA offered the possibility to control the pinhole aperture size and to compare the simulations with the experiment. SEM measurements were important to validate the accuracy of the specified aperture size and eventually to achieve a good agreement between the experiment and the simulation.

The smallest vertical beam sizes were obtained from pinhole apertures in the range of 11 – 23 µm. However, the monochromatic photon flux at the image plane was low and five images had to be acquired to improve the signal to noise ratio. As the aperture size increases, the flux increases whilst the spatial resolution of the pinhole camera decreases.

The experimental data shows a good agreement ($\lesssim 8\%$) with the simulation for the 15 – 47 µm aperture sizes and implies that the pinhole camera system performs as described in the simulation. The remaining discrepancy between simulation and aperture size may be further reduced through optimisation of the simulation and data analysis. Therefore this work could be extended to simulate the broadband PSF for white beam given the known aperture size, thereby removing the need for time-consuming beam measurements of PSF.

Excluding the 11 µm dataset from these measurements and given the white beam spectrum peaks at 23 keV, the optimal aperture size from simulation and experiment for this pinhole camera is approximately 15 µm.

ACKNOWLEDGEMENTS

The authors acknowledge the support of the Karlsruhe Nano Micro Facility (KNMFi) and the KARA synchrotron light source facility at the Karlsruhe Institute of Technology (KIT).

REFERENCES

[1] C. Thomas, G. Rehm, I. Martin, and R. Bartolini, "X-ray pinhole camera resolution and emittance measurement," *Phys. Rev. ST Accel. Beams*, vol. 13, no. 2, p. 022 805, 2010. doi:10.1103/PhysRevSTAB.13.022805

[2] R. Tomás, M. Aiba, A. Franchi, and U. Iriso, "Review of linear optics measurement and correction for charged particle accelerators," *Phys. Rev. Accel. Beams*, vol. 20, p. 054 801, 2017. doi:10.1103/PhysRevAccelBeams.20.054801

[3] P. Elleaume, C. Fortgang, C. Penel, and E. Tarazona, "Measuring beam sizes and ultra-small electron emittances using an X-ray pinhole camera," *J. Synchrotron Radiat.*, vol. 2, no. 5, pp. 209–214, 1995. doi:10.1107/S0909049595008685

ISBN: 978-3-95450-241-7 ISSN: 2673-5350 doi:10.18429/JACoW-IBIC2022-MOP18

[4] E. W. Becker, W. Ehrfeld, P. Hagmann, A. Maner, and D. Münchmeyer, "Fabrication of microstructures with high aspect ratios and great structural heights by synchrotron radiation lithography, galvanoforming, and plastic moulding (LIGA process)," *Microelectron. Eng.*, vol. 4, no. 1, pp. 35–56, 1986. doi:10.1016/0167-9317(86)90004-3

[5] L. M. Bobb, A. F. D. Morgan, and G. Rehm, "Performance Evaluation of Molybdenum Blades in an X-ray Pinhole Camera," in *Proc. IBIC'16*, Barcelona, Spain, Sep. 2016, pp. 795–798. doi:10.18429/JACoW-IBIC2016-WEPG63

[6] A. Rack *et al.*, "Comparative study of multilayers used in monochromators for synchrotron-based coherent hard X-ray imaging," *J. Synchrotron Radiat.*, vol. 17, no. 4, pp. 496–510, 2010. doi:10.1107/S0909049510011623

[7] O. Chubar *et al.*, *Synchrotron radiation workshop.* https://github.com/ochubar/SRW

[8] O. Chubar *et al.*, "Main functions, recent updates, and applications of Synchrotron Radiation Workshop code," in *Advances in Computational Methods for X-Ray Optics IV*, International Society for Optics and Photonics, vol. 10388, 2017, pp. 13–27. doi:10.1117/12.2274285